EARTHQUAKE ENGINEERING AND STRUCTURAL DYNAMICS
Earthquake Engng Struct. Dyn. 2006; **35**:713–736
Published online 10 February 2006 in Wiley InterScience (www.interscience.wiley.com). DOI: 10.1002/eqe.555

Seismic isolation of viaduct piers by means of a rocking mechanism

Yi-Hsuan Chen[1], Wei-Hsin Liao[2], Chien-Liang Lee[2] and Yen-Po Wang[1,*,†]

[1]*Department of Civil Engineering, National Chiao-Tung University, Hsinchu, Taiwan, ROC*
[2]*Natural Hazard Mitigation Research Center, National Chiao-Tung University, Hsinchu, Taiwan, ROC*

SUMMARY

Rocking mechanism can be an effective means of seismic isolation, despite the fact that it is rarely conceived a possible alternative. In this study, the feasibility of utilizing a rocking mechanism for earthquake protection of slender viaduct pier structures is explored both analytically and experimentally. With a discontinuous interface between the pier footings and the underlying pile caps, a rocking system is designed to rock intermittently as the seismic overturning moment exceeds the restoring moment provided by gravity. During the rock mode, the resisting flexural moment in the pier is released while the earthquake load is counteracted by the rotational inertia with respect to the supporting foot, thus preventing the columns from yielding. Analytical modelling of this non-linear dynamic system is derived with a numerical procedure developed based on the fourth-order Runge–Kutta–Nyström method. A series of tests including the free rocking and seismic performance test, has been conducted using a 1:50 scaled-down model structure of a typical viaduct pier system. Both analytical and experimental results show that the rocking pier system (RPS) for seismic protection of viaduct pier structures is effective and stable, and the stronger the earthquake intensity the more pronounced the control efficiency. The concept of using rocking mechanism for seismic isolation of viaduct pier structures has been demonstrated feasible and promising. Nevertheless, practical issues such as prevention of overturning, foot damage due to impact, or possible sliding of the pier following impact need to be carefully dealt with in the design aspect. Copyright © 2006 John Wiley & Sons, Ltd.

KEY WORDS: rocking mechanism; seismic isolation; seismic performance tests

INTRODUCTION

In earthquake-prone areas, slender bridge piers must be designed to withstand substantial lateral loads with sufficient ductility capacity. Viaduct bridges are in general seismically

*Correspondence to: Yen-Po Wang, Department of Civil Engineering, National Chiao-Tung University, 1001 Ta Hsuch Road, Hsinchu, Taiwan, ROC.
†E-mail: ypwang@cc.nctu.edu.tw

Contract/grant sponsor: National Science Council of the Republic of China; contract/grant number: NSC 90-2211-E-009-014

Received 5 April 2005
Revised 26 October 2005
Accepted 30 November 2005

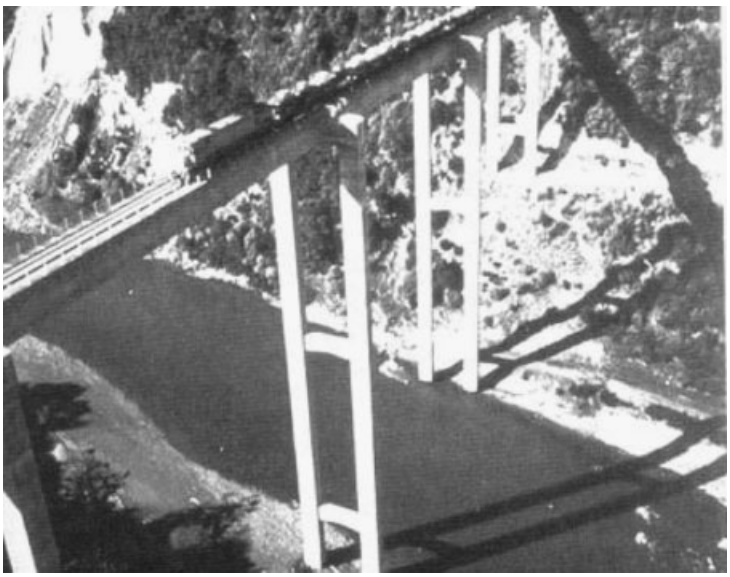

Figure 1. South Rangitikei Viaduct (New Zealand) [6].

weaker in the direction transverse to the bridge axis by resisting the earthquakes with a cantilever (single pier) or narrow-spanned frame system consisting of a cap beam and a couple of columns. To increase reliability of the seismic performance of viaduct piers while reducing the cost demanded by a ductility design, application of structural control techniques becomes a favourable solution. Despite the fact that seismic isolation has been widely accepted as an effective means of structural control for various structural systems, the period-shifting strategy via implementation of flexible or concaved sliding bearings may not be adequate for viaduct piers, however, as their fundamental periods are long in nature.

Free-standing slender structures supported by gravity are easy to uplift, yet the sway with a rocking action has been demonstrated beneficial to reduce seismic responses provided that the problem of overturning at critical conditions can be excluded [1–4]. Rocking mechanism provides a means of seismic isolation by filtering out earthquake energy. With a discontinuous interface between the pier's footing and the underlying pile caps in the transverse direction, the rocking pier system (RPS) is able to rock intermittently as the seismic overturning moment exceeds the restoring moment by gravity. The boundary condition at the footing switches from fixed to hinging as the uplift occurs, with the initial moment-resisting mechanism released instantly. The earthquake load is then counteracted by the rotational inertia of the RPS at the mass centre with respect to the supporting foot. This prevents the piers from yielding and damage. The cost for providing separations at the footings of the piers together with the energy-absorbing devices to prevent overturning could be substantially less than that for providing ductility in the piers and the pile foundation of sufficient depth against uplift, as reported by Beck and Skinner [5]. The first structure that was designed and built with a rocking mechanism for seismic protection is the South Rangitikei Rail Bridge of New Zealand completed in 1981 [6], as shown in Figure 1. The seismic rocking pier system is introduced in the transverse direction of this viaduct bridge for the two most slender piers in the middle.

The RPS is allowed to step with each leg alternately lifting off the pile cap during earthquakes. Moreover, it is facilitated with steel torsional-beam dampers between the separation interfaces to prevent overturning.

The dynamic characteristics of rocking structures are markedly different from those of linearly elastic or ductile structures. The effective natural period of a rigid block in rocking is amplitude-dependent in nature, as proved by Housner [1] in his pioneering work motivated by observing the survival of some water tanks during the 1960 Chilean earthquake. The dynamics of a tank without structural anchorage was modelled as a rigid block in rocking and a linearized equation of motion was derived by assuming small rotation and bouncing-free after impact. Housner's study also indicated that stability of rigid blocks was size-dependent by comparing the responses of two geometrically similar blocks. It was concluded that the larger the block the better the stability. Successive studies by Yim *et al.* [7], Aslam *et al.* [8] and Psycharis and Jennings [9] further explored the effects of slenderness and other parameters on rocking behaviour.

Priestley *et al.* [10] conducted an experimental study on the seismic response of a model structure designed to rock and verified the energy dissipative nature of rocking response predicted by Housner [1]. A response spectrum analysis procedure was also proposed to predict the maximum rocking displacement for single-degree-of-freedom rocking structures. However, as fundamental differences exist between vibration of elastic oscillators and rocking of rigid blocks, Makris and Konstantinidis [11] concluded that the simple spectrum analysis approach by Priestley *et al.* [10] was inherently flawed and inadequate. Huckelbridge and Clough [3] examined experimentally the effect of partial lift-off on a multistorey model structure and confirmed the benefit of uplift action in reducing the strength and ductility demands of the frame. Meek [12] investigated the dynamic response of tipping core-braced buildings using a simplified first-mode model. Parametric studies of tipping core structures were conducted based on a response-spectrum technique. Response spectra of both pulse and earthquake excitations have been derived for various slenderness ratios. It was concluded that for structures with natural frequency between 0.5 and 4 Hz, tipping could reduce the pseudo-acceleration to values considerably less than the fixed-base response, and the reduction is greatest for the most slender structures. Aslam *et al.* [8] investigated the earthquake response of radiation shielding systems used in the particle accelerator laboratory. A series of shaking table tests was conducted to explore the stability of rigid blocks subjected to either harmonic or seismic base excitations. The rocking response and stability of rigid blocks were found sensitive to aspect ratio, block size and coefficient of restitution. The analytical and experimental results under seismic-type input in their study were not well correlated, however.

The objective of this paper is to investigate the feasibility of utilizing rocking mechanism for earthquake protection of viaduct-type structures. The rocking response of deformable structures such as high-piers under seismic load is complicated, as the sticking and rocking phases switch alternately during the transient responses. In this study, the slender high-pier structure is represented by an A-shaped frame exhibiting basic features of RPS as first considered by Beck and Skinner [5]. Analytical modelling of this non-linear dynamic system is derived and a numerical procedure based on the fourth-order Runge–Kutta–Nyström method [13] is developed. A series of tests including free rocking and seismic input has been conducted using a scaled-down A-frame model. The 1940 El Centro earthquake at various intensity levels are used in the shaking table tests. Stability and effectiveness of the RPS in seismic protection of viaduct pier structures are confirmed.

ANALYTICAL MODELLING OF ROCKING PIER SYSTEMS

Rocking response of deformable structures differs from rigid blocks in that the sticking and rocking phases switch alternately during the transient process. Without loss of generality, an A-shaped frame system that exhibits basic features of elastic rocking structures is considered.

Equations of motion

An A-frame of height h and width $2b$ is illustrated in Figure 2 in which R is the length of the pier column and θ_{cr} is the critical angle of rotation beyond which the structure will be subjected to irreversible overturning.

Since the A-frame behaves mechanically more like a truss, it is presumed that the piers remain straight with only axial deformation. In the sticking phases, the RPS deforms elastically with both feet staying in contact with the foundation (or pile cap). The dynamic system is described by the horizontal displacement, u_1, and the vertical displacement, u_2, of the deck at the apex parallel to the global co-ordinate system. In rocking phases, the RPS rocks alternately with one foot uplifted and the other supporting on the foundation as the rotation centre. The dynamic response of the RPS can be resolved into the rigid-body rotation, θ, and the axial deformation, v, along the supporting leg. The rotation angle, θ, is considered positive when the structure rotates about the right foot on O and negative when it rotates about the left foot on O'. It is assumed that the coefficient of friction is sufficiently large to prevent sliding and sliding-rock modes at all time.

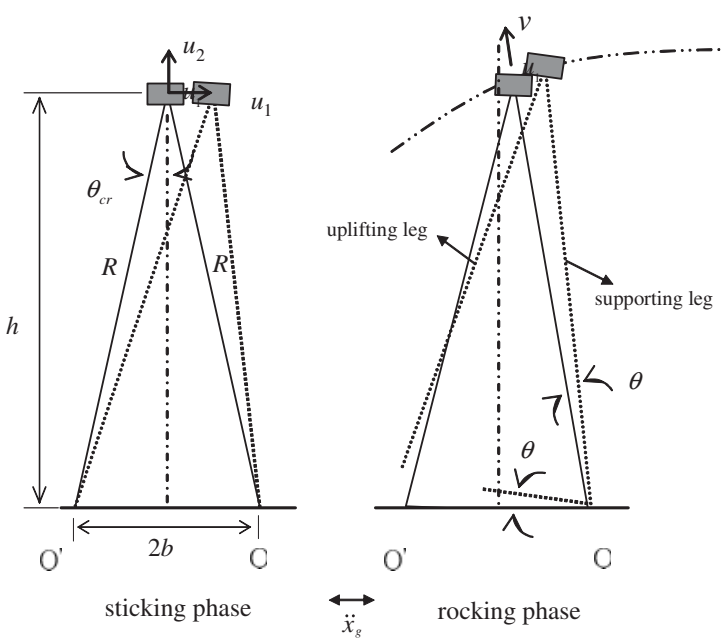

Figure 2. Schematic diagram of the RPS in both the sticking and rocking phases.

Sticking phase

When the axial forces resulted from the weight (static) and the earthquake (dynamic) in both the pier columns are compressive, both feet of the free standing A-frame remain in contact with the foundation and the following inequalities must be satisfied:

$$u_1 \sin\theta_{cr} + u_2 \cos\theta_{cr} \leqslant u_c \tag{1a}$$

and

$$u_1 \sin\theta_{cr} - u_2 \cos\theta_{cr} \geqslant -u_c \tag{1b}$$

where $u_c = R(W + 2P)/2EA\cos\theta_{cr}$ is the critical displacement in which W is the weight of the bridge deck lumped at the apex of the A-frame; P is the weight of each column uniformly distributed over the length; E is the Young's modulus of the material and A is the cross-sectional area of the column.

Under such conditions, the kinematic boundary condition of the RPS at the supports is considered 'fixed' and the RPS responds elastically to the ground excitation. The governing equations of the A-frame RPS under horizontal ground motion $\ddot{x}_g$ can be derived using D'Alembert's principle [14] as

$$\begin{bmatrix} \dfrac{W+(2/3)P}{g} & 0 \\ 0 & \dfrac{W+(2/3)P}{g} \end{bmatrix} \begin{Bmatrix} \ddot{u}_1 \\ \ddot{u}_2 \end{Bmatrix} + \begin{bmatrix} C_{p1} & 0 \\ 0 & C_{p2} \end{bmatrix} \begin{Bmatrix} \dot{u}_1 \\ \dot{u}_2 \end{Bmatrix} + \begin{bmatrix} 2\dfrac{EA}{R}\sin^2\theta_{cr} & 0 \\ 0 & 2\dfrac{EA}{R}\cos^2\theta_{cr} \end{bmatrix} \begin{Bmatrix} u_1 \\ u_2 \end{Bmatrix} = -\begin{Bmatrix} \dfrac{W+P}{g} \\ 0 \end{Bmatrix} \ddot{x}_g \tag{2}$$

where g is the acceleration of gravity; C_{p1} and C_{p2} are the damping coefficients corresponding to u_1 and u_2, respectively.

Onset of uplift

Since a free standing A-frame provides no tension resistance, the RPS starts rocking as the axial forces in one of the pier columns become tensile. The RPS would rock about O with its left foot lifted if

$$u_1 \sin\theta_{cr} + u_2 \cos\theta_{cr} > u_c \tag{3a}$$

and rock about O' with its right foot lifted if

$$u_1 \sin\theta_{cr} - u_2 \cos\theta_{cr} < -u_c \tag{3b}$$

In such circumstances, the kinematic boundary conditions of the RPS at the supports, O or O' alternately, are considered 'hinged'.

Rocking phase

Provided that the RPS rocks within the critical angle, the equation of motion can be derived as

$$I_o\ddot{\theta} + \mathrm{sgn}(\theta)\left[\left(W + \frac{P}{2}\right)R\sin(\theta_{\mathrm{cr}} - |\theta|) + P\left[b\cos\theta + \frac{R}{2}\sin(\theta_{\mathrm{cr}} - |\theta|)\right]\right]$$
$$+ \left[\left(\frac{W + P/2}{g}\right)R\cos(\theta_{\mathrm{cr}} - |\theta|) + \left(\frac{P}{g}\right)\left[b\sin\theta + \frac{R}{2}\cos(\theta_{\mathrm{cr}} - |\theta|)\right]\right]\ddot{x}_{\mathrm{g}} = 0 \quad (4a)$$

$$\left(\frac{W + 4P/3}{g}\right)\ddot{v} + \left(\frac{EA}{R}\right)v + \left(\frac{W + 2P}{2}\right)\cos(\theta_{\mathrm{cr}} - |\theta|)$$
$$- \mathrm{sgn}(\theta)\left(\frac{W + 4P/3}{g}\right)\ddot{x}_{\mathrm{g}}\sin(\theta_{\mathrm{cr}} - |\theta|) = 0 \quad (4b)$$

where $I_o = [W + (2/3)P]R^2 + 2Pb^2/g$ is the rotational moment of inertia about the supporting foot.

If the damping of the pier column corresponding to the axial degree of freedom is assumed viscous and denoted C_{pr}, and the rotation angle, θ, of the RPS is considered to be much smaller than θ_{cr}, that is, $\theta_{\mathrm{cr}} - |\theta| \approx \theta_{\mathrm{cr}}$, then the governing equation can be further simplified as

$$\begin{bmatrix} I_o & 0 \\ 0 & \dfrac{W + (4/3)P}{g} \end{bmatrix}\begin{Bmatrix}\ddot{\theta}\\ \ddot{v}\end{Bmatrix} + \begin{bmatrix} 0 & 0 \\ 0 & C_{pr}\end{bmatrix}\begin{Bmatrix}\dot{\theta}\\ \dot{v}\end{Bmatrix} + \begin{bmatrix} \dfrac{Pb}{g}\ddot{x}_{\mathrm{g}} & 0 \\ 0 & \dfrac{EA}{R}\end{bmatrix}\begin{Bmatrix}\theta\\ v\end{Bmatrix}$$
$$= -\begin{Bmatrix} \mathrm{sgn}(\theta)(W + 2P)b \\ \left(\dfrac{W + 2P}{2}\right)\cos\theta_{\mathrm{cr}}\end{Bmatrix} - \begin{Bmatrix} \left(\dfrac{W + P}{g}\right)h \\ -\mathrm{sgn}(\theta)\dfrac{W + (4/3)P}{g}\sin\theta_{\mathrm{cr}}\end{Bmatrix}\ddot{x}_{\mathrm{g}} \quad (5)$$

A numerical procedure for the non-linear analysis of the rocking system is developed in this study based on the fourth-order Runge–Kutta–Nyström method.

Determination of phase-switch and the corresponding initial conditions

Rocking mode of the RPS commences as one of the column's axial stresses calculated from Equation (3) becomes tensile, as discussed previously. After the rocking mode starts, impacts occur intermittently due to re-contact of the lifted column foot onto the rigid foundation. Then the RPS is in transition from rocking to sticking, or proceeds to rock without sticking in place if the resulting overturning moment exceeds the restoring moment provided by gravity.

Essential to authentically simulating the rocking responses is to identify the timing at which the impacts occur, and determine the associated initial conditions that assure continuity of the responses consistent with the motion conditions.

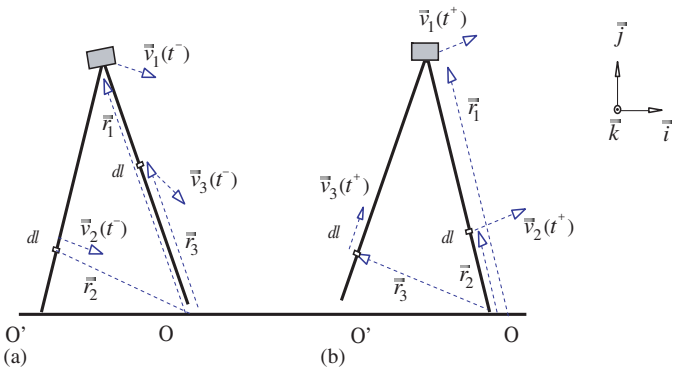

Figure 3. Angular velocity of an RPS prior to and after impact: (a) before impact; and (b) after impact.

Impacts occur whenever the rotation angle reaches zero during the rocking phase. Therefore, the time for phase-switch can be determined by solving

$$\theta(t) = 0 \tag{6}$$

using the Newton–Raphson method [15]. Strategy in the dynamic analysis is to first assume the RPS shifts to the sticking phase immediately after the impact, thus Equation (2) governs the motion condition. The initial states at the very time instant after impact (t^+) resolved from Equation (6) are then determined in accordance with the conservation of linear momentum in the horizontal direction as

$$\dot{u}_1(t^+) = h\dot{\theta}(t^-) \tag{7a}$$

and

$$\dot{u}_2(t^+) = 0 \tag{7b}$$

where a perfect inelastic collision in the vertical direction is assumed. Condition (1) must be satisfied if the presumed motion condition is true. Otherwise, the RPS should continue to rock, and Equations (4) or (5) should be applied with the corresponding initial velocities for the rocking response redefined.

As illustrated in Figure 3(a), the angular momentum of the RPS with respect to O right before the impact (at $t = t^-$) is expressed as

$$\begin{aligned}
\mathbf{H}_O(t^-) &= \sum_{i=1}^{3} \mathbf{r}_i \times M_i \mathbf{v}_i(t^-) \\
&= (-b\mathbf{i} + h\mathbf{j}) \times \left(\frac{W}{g}\right) \dot{\theta}(t^-)(h\mathbf{i} - b\mathbf{j}) \\
&\quad + \int_0^R [(-2b + l\sin\theta_{cr})\mathbf{i} + l\cos\theta_{cr}\mathbf{j}] \times \left(\frac{P}{Rg}\right) \dot{\theta}(t^-)(l\cos\theta_{cr}\mathbf{i} - l\sin\theta_{cr}\mathbf{j})\,\mathrm{d}l \\
&\quad + \int_0^R (-l\sin\theta_{cr}\mathbf{i} + l\cos\theta_{cr}\mathbf{j}) \times \left(\frac{P}{Rg}\right) \dot{\theta}(t^-)[l\cos\theta_{cr}\mathbf{i} - (2b - l\sin\theta_{cr})\mathbf{j}]\,\mathrm{d}l \\
&= -\left[\left(\frac{W}{g}\right)(h^2 - b^2) + \left(\frac{2P}{3g}\right)(b^2 + h^2)\right] \dot{\theta}(t^-)\mathbf{k}
\end{aligned} \tag{8a}$$

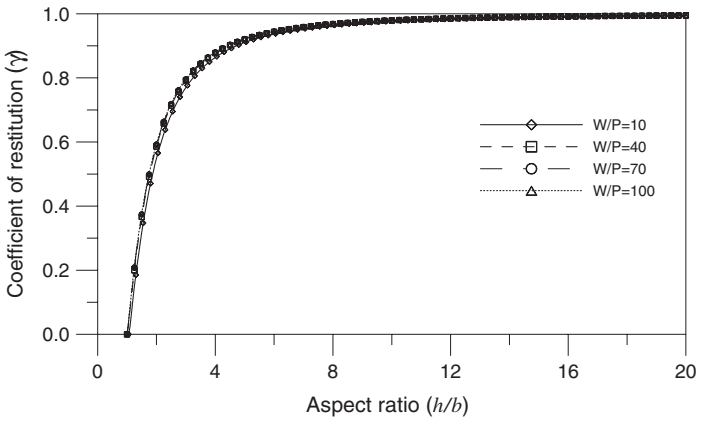

Figure 4. Variation of coefficient of restitution with respect to aspect ratio.

where $\mathbf{r}_i$ is the position vector originated from O to each component (deck, right pier column, and left pier column) of the RPS, and $\mathbf{v}_i$ is the corresponding tangential velocity.

Similarly, the angular momentum of the RPS with respect to O right after the impact (at $t = t^+$), as illustrated in Figure 3(b), is expressed as

$$\begin{aligned}\mathbf{H}_O(t^+) &= \sum_{i=1}^{3} \mathbf{r}_i \times M_i \mathbf{v}_i(t^+) \\ &= (-b\mathbf{i} + h\mathbf{j}) \times \left(\frac{W}{g}\right)(h\dot{\theta}(t^+)\mathbf{i} + b\dot{\theta}(t^+)\mathbf{j}) \\ &\quad + \int_0^R (-l\sin\theta_{\mathrm{cr}}\mathbf{i} + l\cos\theta_{\mathrm{cr}}\mathbf{j}) \times \left(\frac{P\dot{\theta}(t^+)}{Rg}\right)[l\cos\theta_{\mathrm{cr}}\mathbf{i} + l\sin\theta_{\mathrm{cr}}\mathbf{j}]\,\mathrm{d}l \\ &\quad + \int_0^R [(-2b + l\sin\theta_{\mathrm{cr}})\mathbf{i} + l\cos\theta_{\mathrm{cr}}\mathbf{j}] \times \left(\frac{P\dot{\theta}(t^+)}{Rg}\right)[l\cos\theta_{\mathrm{cr}}\mathbf{i} + (2b - l\sin\theta_{\mathrm{cr}})\mathbf{j}]\,\mathrm{d}l \\ &= -\left[\left(\frac{W}{g}\right)(b^2 - h^2) + \left(\frac{P}{3g}\right)(2h^2 + 8b^2)\right]\dot{\theta}(t^+)\mathbf{k} \end{aligned} \tag{8b}$$

Based on the principle of conservation of angular momentum, the coefficient of restitution, γ, defined as the ratio of angular velocity after the impact at time t^+ to that prior to the impact at time t^-, can be written as

$$\gamma = \frac{\dot{\theta}(t^+)}{\dot{\theta}(t^-)} = \frac{\left(\frac{W}{P}\right)\left[\left(\frac{h}{b}\right)^2 - 1\right] + \frac{2}{3}\left[\left(\frac{h}{b}\right)^2 + 1\right]}{\left(\frac{W}{P}\right)\left[\left(\frac{h}{b}\right)^2 + 1\right] + \frac{1}{3}\left[2\left(\frac{h}{b}\right)^2 + 8\right]} \tag{9}$$

Therefore, the angular velocity $\dot{\theta}(t^+) = \gamma\dot{\theta}(t^-)$ will be considered as the initial velocity at the next phase of rocking.

Figure 4 shows the coefficient of restitution, γ, with respect to the aspect ratio, h/b, for various mass ratios ($W/P = 10$, 40, 70 and 100). The coefficient of restitution approaches

unity for extremely slender structures and drops to nearly zero for squatty ones as h/b ratio is close to one. Moreover, the coefficient of restitution is found insensitive to the mass ratio between the deck and pier.

DYNAMIC CHARACTERISTICS OF ROCKING PIER SYSTEMS

In order to gain more insight of the dynamic characteristics of the RPS, the dynamic response of the RPS with various aspect ratios is investigated under free rocking and harmonic ground excitation. It is assumed that the damping coefficients C_{p1}, C_{p2} and C_{pr} are ignored in the analyses. Moreover, the integration time-step considered in the numerical analysis is 0.0025 s.

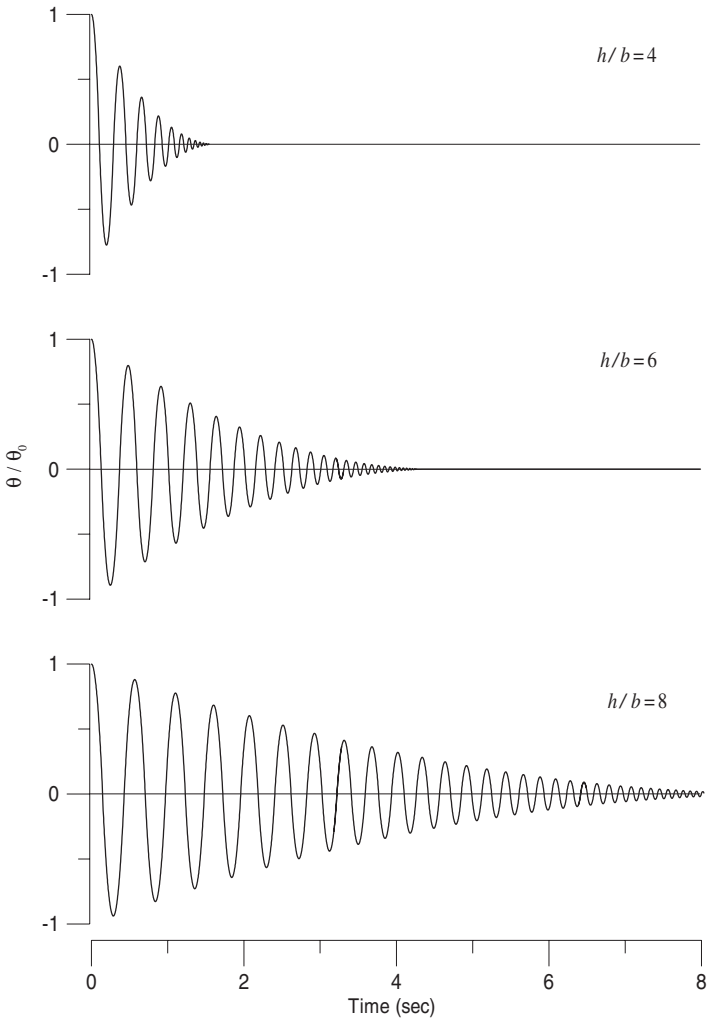

Figure 5. Free rocking responses of RPS with respect to various aspect ratios ($\theta_0/\theta_{cr} = 0.1$).

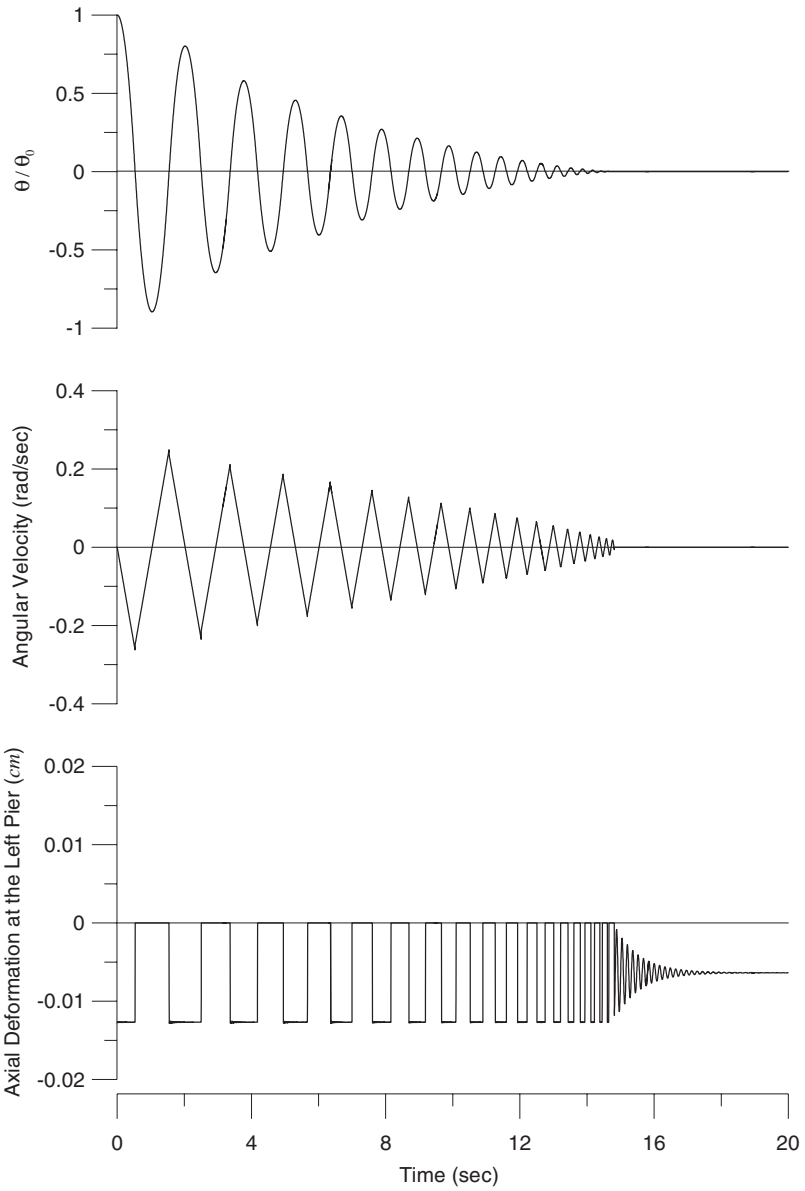

Figure 6. Free rocking responses of RPS ($\theta_0/\theta_{cr} = 0.32, h/b = 10$).

Free rocking responses

Figure 5 illustrates the free rocking responses of the RPS with aspect ratio $h/b = 4$, 6 and 8, respectively. The RPS is released at an initial position, θ_0, of one-tenth of the corresponding critical angle, θ_{cr}. The responses decay asymptotically despite the fact that no structural

damping is specified, indicating that rocking mechanism along is energy dissipative. The energy dissipative capability of the RPS, however, decreases as the aspect ratio increases. Moreover, it is observed that the effective period of the RPS is strongly dependent on the rocking amplitude. The cycling time of the rocking response becomes shorter and shorter as the amplitude reduces in the time frame before the structure is finally at rest. These phenomena agree with the free rocking response of rigid blocks reported by Housner [1].

The free rocking response for an RPS with $h/b = 10$ released at $\theta_0 = 0.32\theta_{cr}$ is shown in Figure 6. The angular velocity appears to vary linearly between two consecutive impacts, implying a constant angular acceleration of rocking. The axial deformation of the left column is either compressive or zero as lifted. Oscillation of the axial deformation continues in the sticking mode and decays asymptotically to the position of static equilibrium.

Harmonic excitations

The forced oscillation of an RPS and its fixed-base counterpart under harmonic ground motion are compared in Figure 7. The driving frequency of the excitation is deliberately chosen to coincide with the natural frequency of the base-fixed pier. It is evident that both the horizontal

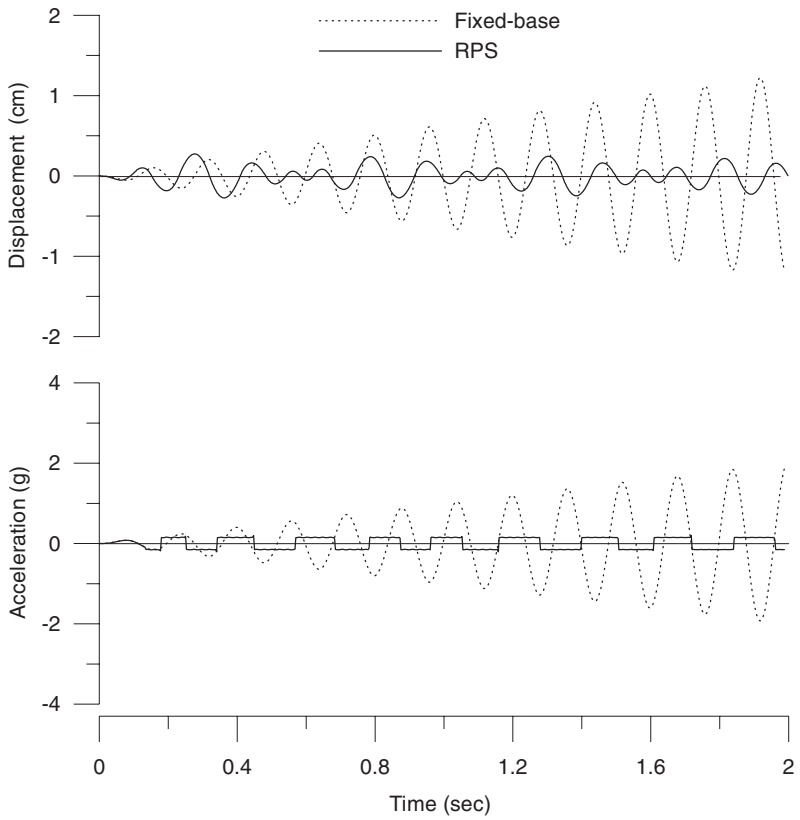

Figure 7. Comparison of harmonic responses of RPS with conventional structures.

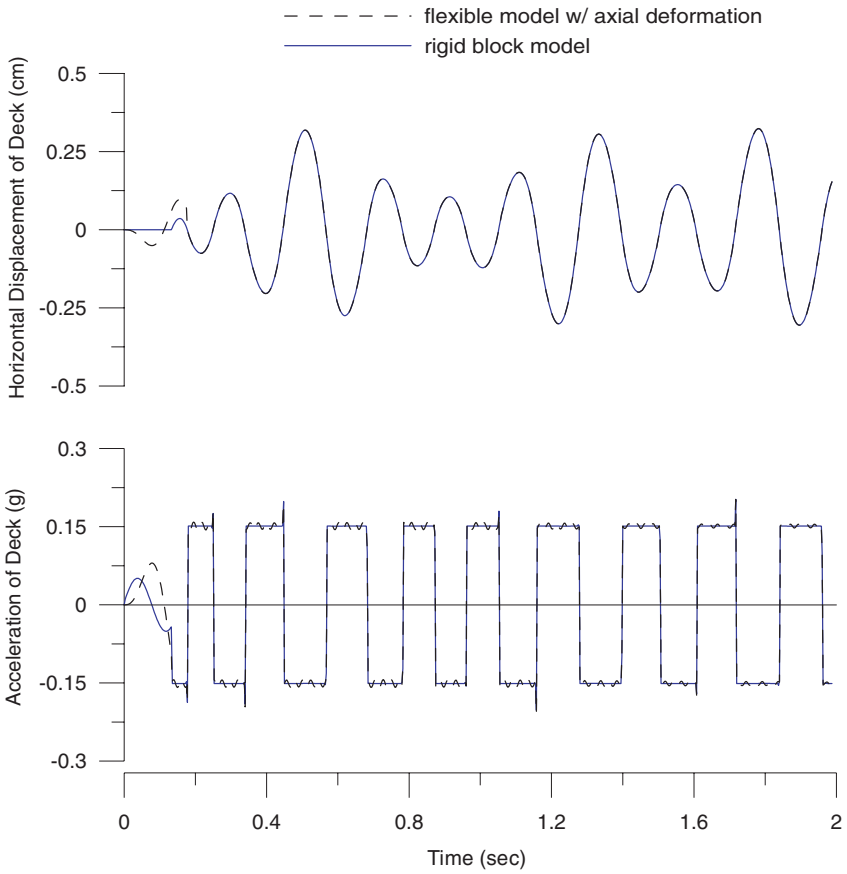

Figure 8. Comparison of results by different analytical models (harmonic excitation).

displacement and acceleration of the deck for the base-fixed pier divert with time due to resonance, while those for the RPS are evidently bounded. The horizontal displacement and acceleration of the deck under harmonic excitation derived by using both the rigid model and flexible model with axial deformation are compared in Figure 8. The deck displacements obtained from both analytical models are barely the same except the transient part where the rigid block remains still. The acceleration responses by both models predict the same track, in large, except that the flexible model gives some wavelets around the plateau of the response.

Structures having specific natural frequencies may have chance resonating with the input excitation at the overlapping of frequency contents. Resonance of rocking systems with the input excitation does not occur, however, as the amplitude-dependent oscillating frequency never is locked in at any specific frequency. This feature of rocking mechanism may be advantageous for seismic isolation. Nevertheless, unless some forms of lateral constraint can be provided for prevention of overturning, the issue of structural stability for free standing rocking pier systems cannot be overlooked. As an example, the rocking response of a slender RPS with an aspect ratio of 5 under a harmonic ground excitation with a period of two-second

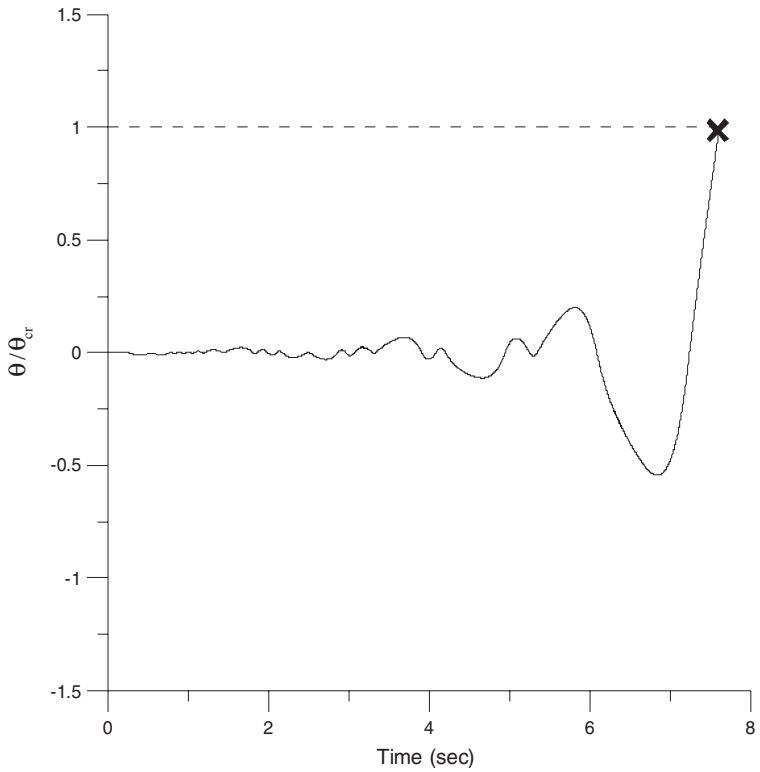

Figure 9. Rotational angle of RPS under a long-period harmonic ground motion.

is examined. In Figure 9, the rotational angle of the RPS grows, before the steady state is reached, to its critical angle (θ_{cr}), implying overturning of the system.

EXPERIMENTAL VERIFICATIONS

As a further step in justifying the theory of rocking mechanism, a series of dynamic tests including the free rocking and seismic shaking table tests has been conducted in the lab. A model structure in the similitude of a prototype viaduct pier is designed in accordance with Buckingham's theory [16] to reserve geometrical and dynamic similarities simultaneously. Effectiveness of the rocking mechanism for earthquake protection of viaduct piers is examined via shaking table tests using the 1940 El Centro earthquake as input.

Experimental setup

Model structure. A 1:50 scaled A-frame modal structure of a prototype 100-meter-high, slender (aspect ratio $h/b = 10$) reinforced concrete viaduct pier is fabricated for the tests. In addition to geometrical similarity, the consistency of acceleration responses between the model and the prototype is considered as the design target. The rest of the modal parameters

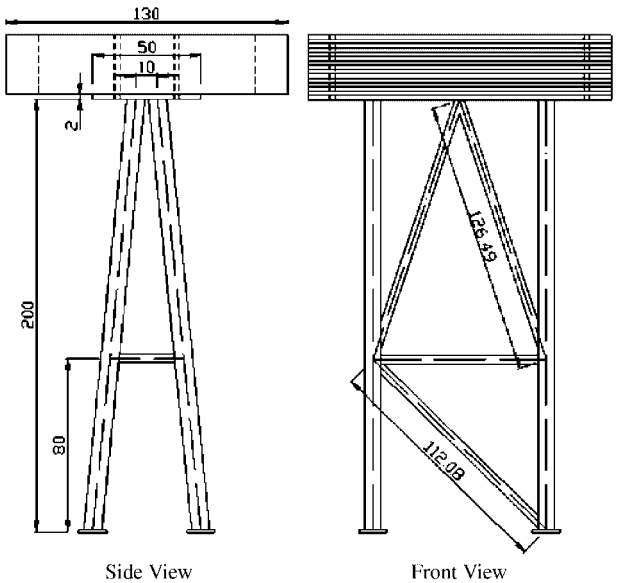

Figure 10. Schematic diagram of the A-frame model (Unit: cm).

Table I. Structural parameters.

	Prototype pier	Scaled model
Height of the pier (m)	100	2
Base-width of the pier (m)	20	0.4
Area of the pier (m^2)	2.7731	0.00111
Weight of deck (N)	6.7×10^6	1.789×10^4
Weight of the pier (N)	6.56×10^6	1.712×10^2
Stiffness of the pier (N/m)	8.4×10^8	1.12×10^8
Density of the material (kg/m^3)	2400	7850
Young's modulus (Gpa)	30.44	203
Natural frequency (Hz)	0.611	4.89
Sampling time scale (s)	0.02	0.0025

(weight of deck, time scaling, natural frequency, etc.) are then determined in accordance with Buckingham's theory [16]. The modal structure, as illustrated in Figure 10, consists primarily of steel tubes, with steel plates assembled on top of the A-frame to achieve the desired weight of the deck. The total weight of the model is about 1.8×10^4 N. The height of the double A-frame model is 2 m and its width at the base in the direction of ground motion is 0.4 m. In order to simulate a pure rocking condition of the modal structure, steel angles were anchored on the pedestal against each of the footings to prevent slippage during the tests. The dimensions of the prototype pier and the scaled model are summarized in Table I. Figure 11 shows the double A-frame model structure resting on the shaking table.

Figure 11. The modal structure on shaking table.

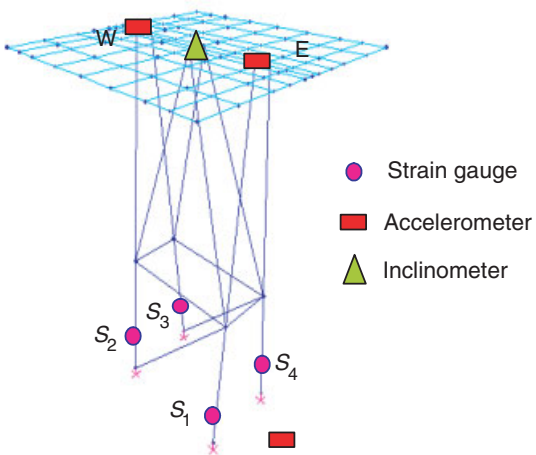

Figure 12. Instrumentations of the modal structure.

Instrumentations and test programs. The rotational velocity, acceleration of the deck and axial strains of the pier columns are representative rocking responses to be measured using inclinometer, accelerometers and strain gauges, respectively. Locations of the transducers in the test setup are specified in Figure 12. A sampling rate of 100 Hz was considered in data acquisition.

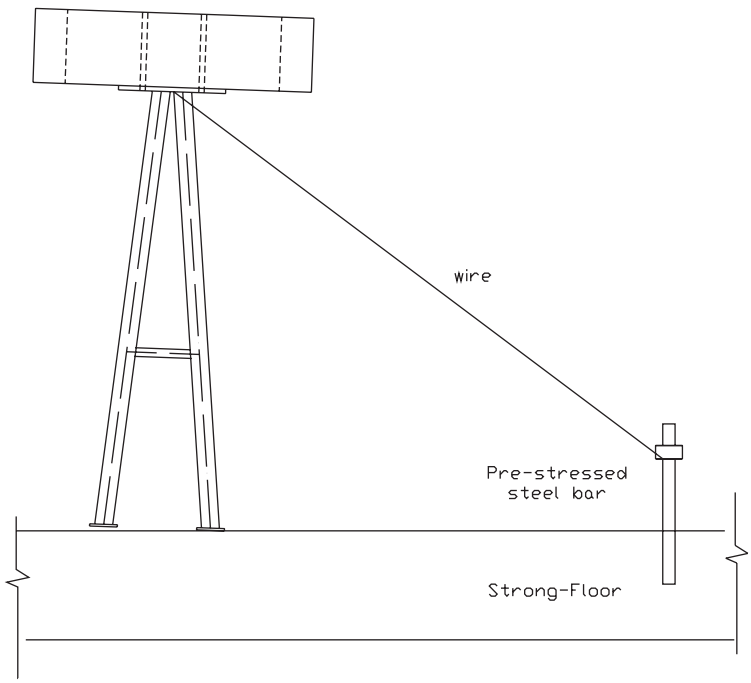

Figure 13. Illustrative diagram for the setup of free rocking tests.

The tests conducted in this experimental study include the free rocking tests and earthquake simulation tests. The objective of the free rocking tests is to shed light on the fundamental characteristics of the rocking mechanism, in particular, the amplitude-dependent cycling frequency and energy-dissipative nature predicted by the theory previously derived. The objective of the earthquake simulation tests is to verify the feasibility of using the rocking mechanism as a means of seismic isolation for protection of viaduct-type bridge piers under severe earthquakes. The model A-frame was also tested with its footings bolted to the foundation to simulate the conventional pier structure. The recorded seismic responses were compared with those of the rocking system and utilized for system identification of the modal structure.

Free rocking tests. The free rocking tests were conducted by imposing an initial angular displacement to the modal A-frame at $\theta_0/\theta_{cr} = 0.32$ and 0.40, respectively. During the test, the free standing A-frame was pulled laterally with a wire tied below the deck to the desired position with the other end of the wire tied to a rod, as illustrated in Figure 13. The structure was released for rocking from the initial position by cutting off the wire instantly. The data acquisition system was triggered prior to releasing of the structure.

The angular velocity responses recorded in the free rocking test with $\theta_0/\theta_{cr} = 0.32$ is illustrated in Figure 14. The analytical prediction of the responses with a coefficient of restitution $\gamma = 0.95$ agrees very well with the experimental results. It is noted that the coefficient of restitution was calculated by Equation (9) based on $b = 0.32$ m rather than 0.20 m to reflect the distance between the outer edges (the actual rotation centre O and O') of the extension

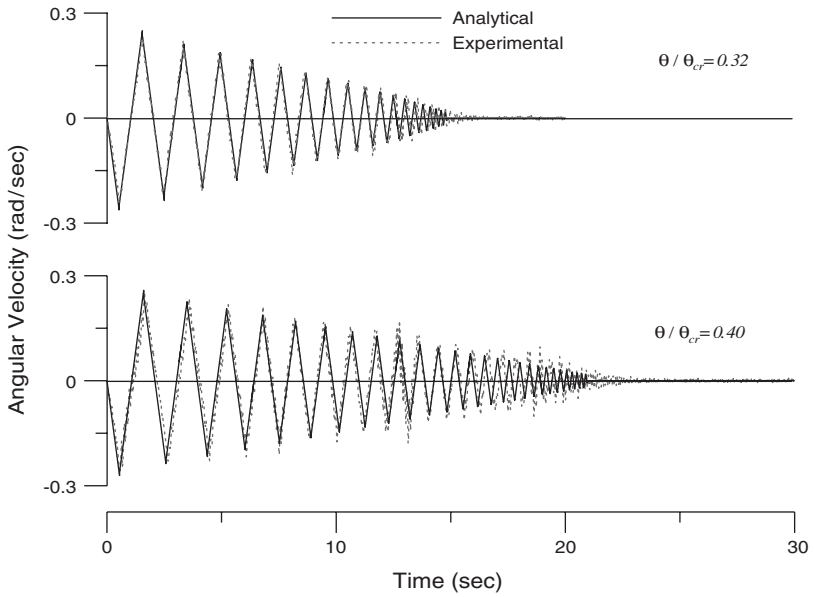

Figure 14. Comparison of angular velocity in free rocking.

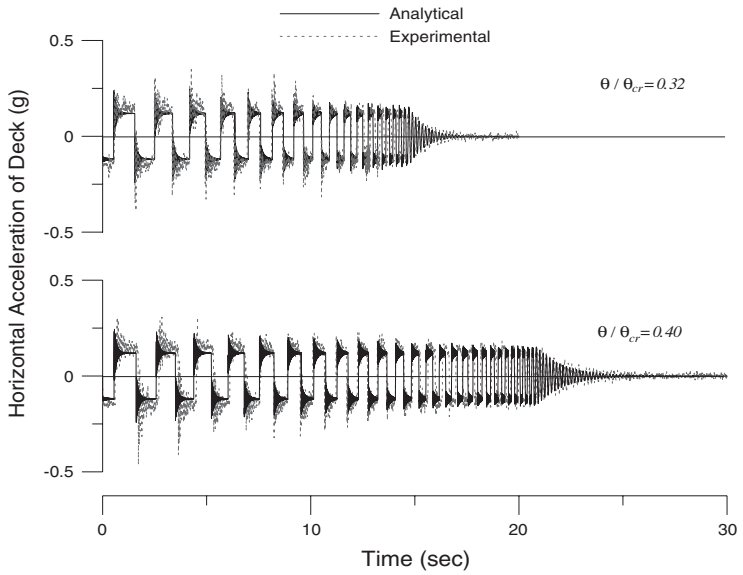

Figure 15. Comparison of deck acceleration in free rocking.

plates at the footings. Figure 15 shows the deck acceleration responses in the horizontal direction. High frequency responses contributed by the axial acceleration due to impact oscillate around a plateau corresponding to the projective component of the tangential acceleration,

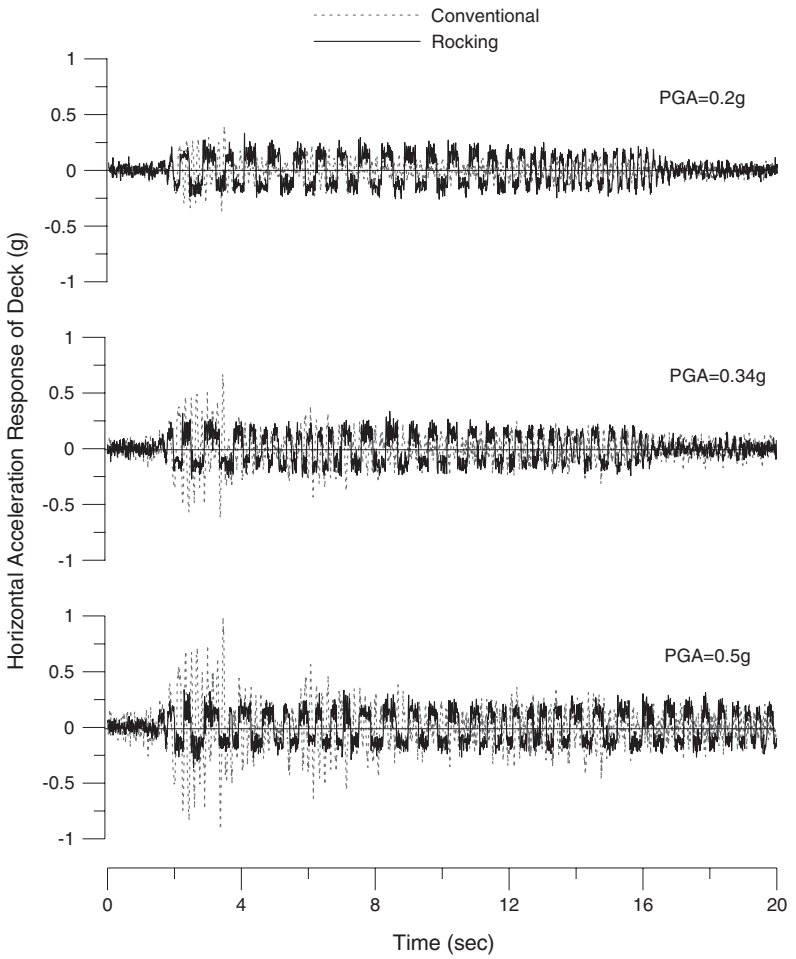

Figure 16. Comparison of deck accelerations under El Centro Earthquake.

$\bar{h}\ddot{\theta}$, in which $\bar{h}$ is the height of the model measured from the base to the top of the deck, and $\ddot{\theta}$ the angular acceleration equal to the slope of the angular velocity between two consecutive impacts. It is also observed that vibration of the deck lasts a little while in a sticking condition after the rocking mode stops. The damping of the model in the stick condition was estimated to be 1.96% via system identification analysis. Good correlation between the analytical and experimental results has been observed.

The results for $\theta_0/\theta_{cr} = 0.40$ is illustrated in Figures 14–15. Similar phenomena have been observed. The amplitudes of the angular velocity and acceleration appear to be insensitive to the initial condition. The only difference is that the case with a larger initial angular displacement decays slower. The analytical and experimental results agree very well with each other in all cases consistently. Adequacy of the proposed theory and numerical procedure is confirmed.

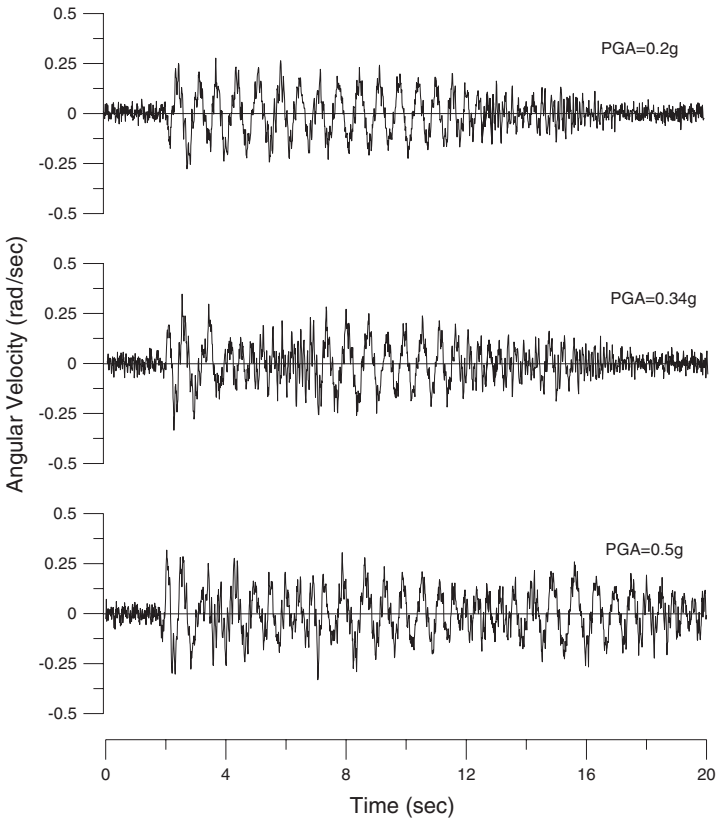

Figure 17. Angular velocity responses of the RPS under El Centro Earthquake.

Earthquake simulation tests. The model structure was first tested in a base-fixed condition using the El Centro earthquake. To avoid yielding in the pier columns, the intensity of the earthquake was scaled to PGA = 0.2 g in the test. The test results served as the basis for comparison with the rocking system. Acceleration responses of the deck and the shaking table were to be used in system identification analysis. A stochastic adaptive filtering technique was adopted considering a single-input–single-output (SISO) auto-regressive (ARX) model [17]. The natural frequency and the damping ratio of the modal structure were identified to be 6.39 Hz and 1.96%, respectively.

Performance assessment of RPS for seismic isolation. The model in a free-standing condition was tested under El Centro earthquake with its intensity scaled, from 0.2 up to 0.5 g, to verify the feasibility of the rocking mechanism under rigorous conditions. No overturning occurred even at the most critical test condition (PGA = 0.5 g).

Figure 16 illustrates the measured deck acceleration responses of the model structure under different PGA levels. It is evident that a significant reduction can be achieved if the structural base has been allowed to uplift as compared with its base-fixed counterpart, referred

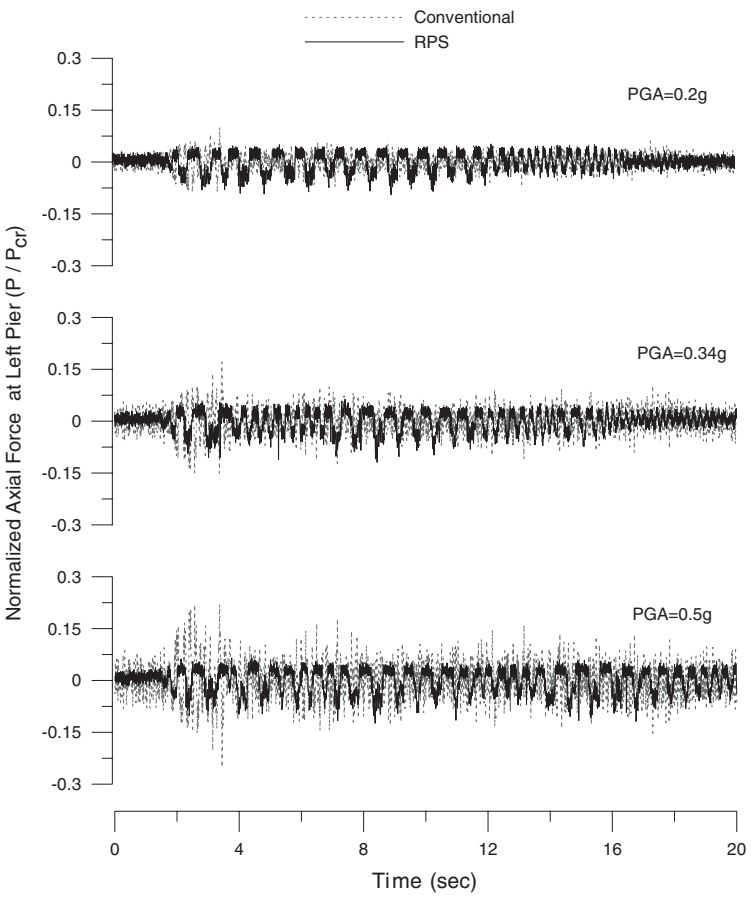

Figure 18. Comparison of the axial forces at the left pier under El Centro Earthquake.

to as the conventional model herein. In the extreme case with PGA = 0.5 g, the peak reduction is 64% for deck acceleration. The acceleration responses increase linearly with the intensity for the conventional one while reaching a certain threshold at nearly 0.35 g for the rocking system, regardless of the PGA levels. This reveals the effectiveness of the rocking mechanism as a safety 'fuse' for seismic structures. Furthermore, the angular velocity responses shown in Figure 17 differ insignificantly in their magnitudes under different intensity levels.

The axial force of the pier converted from the strain measurement and normalized with respect to the critical load, P_{cr}, is shown in Figure 18. Evidently, significant reduction in the axial forces of the RPS has been achieved as compared with those for the conventional type. In the most extreme case (PGA = 0.5 g), a peak reduction of 52% has been achieved. It is noted that the stress in the RPS should be non-positive all the time. The tensile force observed in the responses, however, was caused by the strain measurement relative to the neutral state of the static equilibrium at which the strain gauge was attached.

Table II. Effectiveness assessment of RPS.

Intensity	PGA = 0.2 g			PGA = 0.34 g			PGA = 0.5 g		
Structural type	Conventional	RPS	Reduction (%)	Conventional	RPS	Reduction (%)	Conventional	RPS	Reduction (%)
Max response quantities*									
$\ddot{u}_h(g)$	0.40	0.33	18	0.67	0.34	49	0.99	0.36	64
v_p/v_{cr}	3.3	1	69	5.5	1	82	8.1	1	88
OM/OM_{cr}	4.0	1	75	6.7	1	85	9.9	1	90
θ/θ_{cr}	—	0.20	—	—	0.24	—	—	0.25	—
P/P_{cr} Compression	0.09	0.09	0	0.15	0.12	20	0.25	0.12	52
Tension	0.10	—	—	0.17	—	—	0.22	—	—

$\ddot{u}_h$ = Horizontal acceleration of deck; v_p/v_{cr} = axial deformation of pier (Normalized with respect to critical deformation); OM/OM_{cr} = overturning moment (Normalized with respect to restoring moment due to gravity); θ/θ_{cr} = angular displacement (Normalized with respect to critical angle); P/P_{cr} = Normalization axial force of pier.

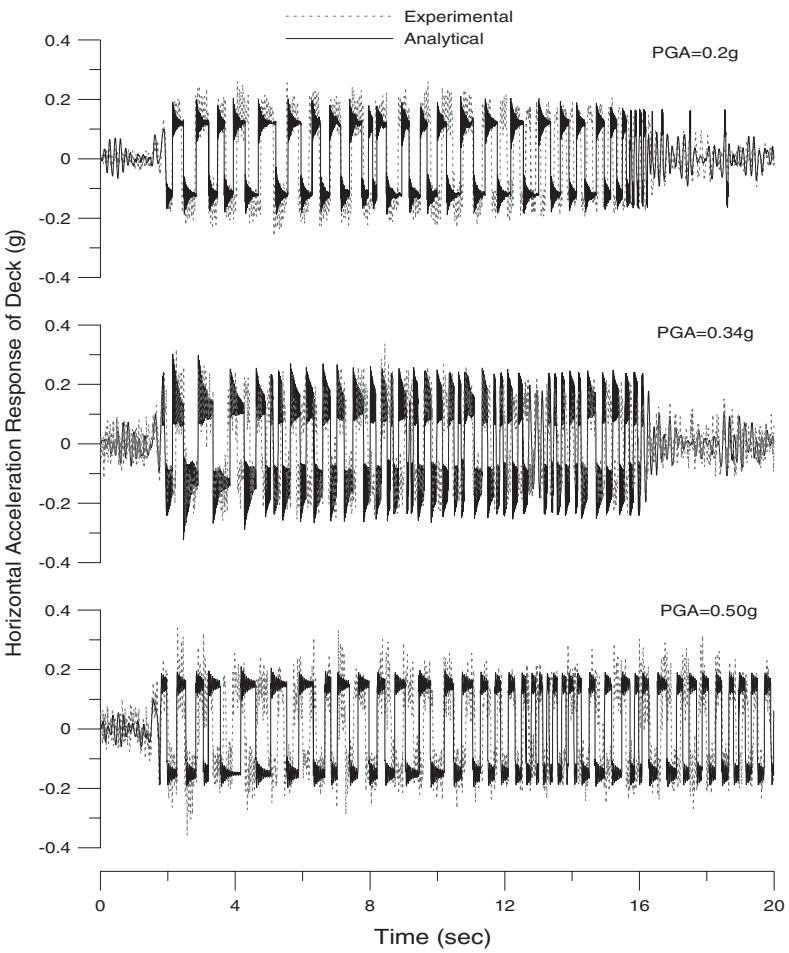

Figure 19. Comparison of deck accelerations under El Centro Earthquake.

Assessment of the test results for the RPS in comparison with the conventional model is summarized in Table II. Evidently, the RPS performs significantly better than the conventional one. Over 70% of the peak reduction in the axial deformation of the pier has been achieved. Also, the overturning moment has been significantly reduced. At the most critical test conditions (PGA = 0.5 g), reduction of the maximum overturning moment of 90% has been obtained. Moreover, it has been shown that the stronger the earthquake intensity, the better the control effects. The effectiveness of rocking mechanism for isolation of high-pier bridges is confirmed.

Comparison of the experimental and analytical results is illustrated in Figure 19 for the acceleration response and Figure 20 for the angular velocity at various PGA levels of the input motion. The analytical predictions of the horizontal acceleration and angular velocity follow closely the waveforms of the experimental data.

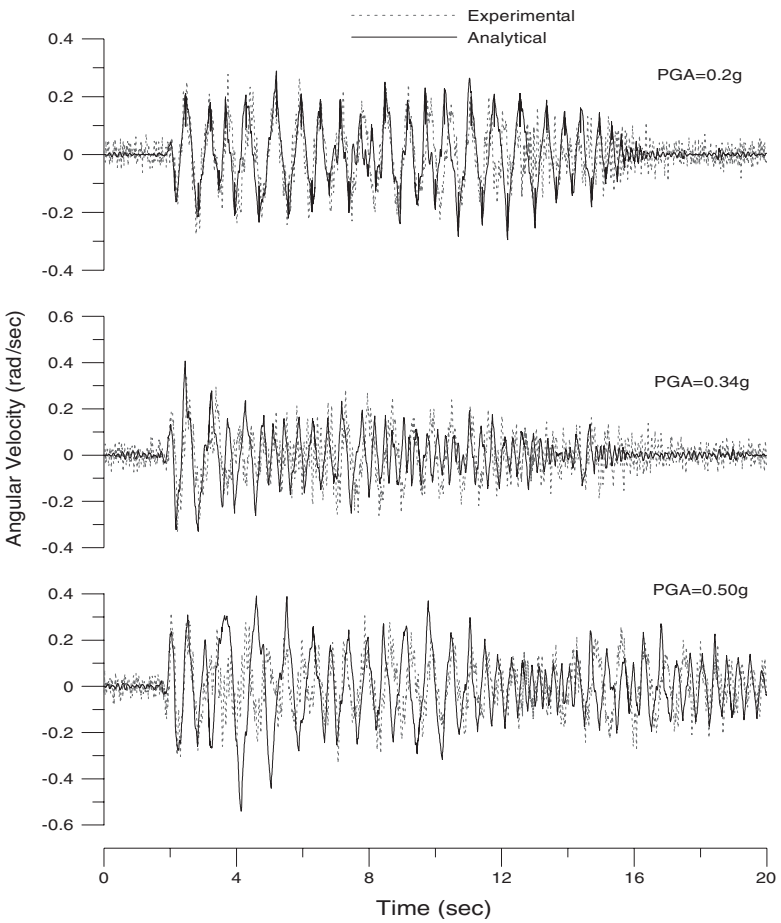

Figure 20. Comparison of angular velocities under El Centro Earthquake.

CONCLUSIONS

In this study, the feasibility of utilizing rocking mechanism for earthquake protection of viaduct-type structures has been explored both analytically and experimentally. The amplitude-dependent cycling time and energy-dissipative nature of rocking mechanism has been derived analytically and observed in the free rocking tests. The coefficient of restitution derived theoretically matches closely with the test results. Significant reduction of seismic responses has been observed for the structures designed to rock. Moreover, stability and effectiveness of the RPS in dynamic response alleviation under severe earthquakes have been confirmed via shaking table tests. It has been observed from the series of tests that, the stronger the earthquake intensity the better the control efficiency. This is attributed to the non-linear characteristics of the rocking mechanism that, regardless of the earthquake intensity, the seismic force is limited to a threshold beyond which the RPS would rock at a constant angular acceleration.

The proposed analytical modelling and solution algorithm for dynamic analysis of rocking systems has been sufficient. Nevertheless, practical issues such as prevention of overturning, foot damage due to impact, or possible sliding of the pier following impact need to be carefully dealt with in the design aspect.

ACKNOWLEDGEMENTS

This research is sponsored by the National Science Council of the Republic of China under Grant no. NSC90-2211-E-009-014.

REFERENCES

1. Housner GW. The behavior of inverted pendulum structures during earthquake. *Bulletin of the Seismological Society of America* 1963; **53**(2):403–417.
2. Meek JW. Effects of foundation tipping on dynamic response. *Journal of the Structural Division* (ASCE) 1975; **101**(ST7):1297–1311.
3. Hukelbridge AA, Clough RW. Seismic response of uplifting building frame. *Journal of the Structural Division* (ASCE) 1978; **104**(ST8):1211–1229.
4. Chopra AK, Yim CS. Simplified earthquake analysis of structures with foundation uplift. *Journal of the Structural Engineering* (ASCE)1985; **111**(4):906–930.
5. Beck JL, Skinner RI. The seismic response of a reinforced concrete bridge pier designed to step. *Earthquake Engineering and Structural Dynamics* 1974; **2**:343–358.
6. Skinner RI, Robinson WH, McVerry GH. *An Introduction to Seismic Isolation*. Wiley: Chichester, 1993.
7. Yim CS, Chopra AK, Penzien J. Rocking response of rigid blocks to earthquake. *Earthquake Engineering and Structural Dynamics* 1980; **8**:565–587.
8. Aslam M, Godden WG, Scalise DT. Earthquake rocking response of rigid bodies. *Journal of the Engineering Mechanics Division* (ASCE) 1980; **106**:377–392.
9. Psycharis IN, Jennings PC. Rocking of slender rigid bodies allowed to uplift. *Engineering and Structural Dynamics* 1983; **11**:57–76.
10. Priestley MJN, Evison RJ, Carr AJ. Seismic response of structures free to rock on their foundations. *Bulletin of the New Zealand National Society for Earthquake Engineering* 1978; **11**(3):141–150.
11. Makris N, Konstantinidis D. The rocking spectrum and the limitations of practical design methodologies. *Engineering and Structural Dynamics* 2003; **32**:265–289.
12. Meek JW. Dynamic response of tipping core buildings. *Earthquake Engineering and Structural Dynamics* 1978; **6**:437–454.
13. Craig Jr. RR. *Structural Dynamics—An Introduction to Computer Methods*. Wiley: New York, 1981.
14. Chopra AK. *Dynamics of Structures—Theory and Applications to Earthquake Engineering*. Prentice-Hall: Englewood Cliffs, NJ, 1995.
15. Borse GJ. *Numerical Methods with MATLAB: A Resource for Scientists and Engineers*. PWS Publishing: Boston, 1997.
16. Hossdrof Heinz. *Model Analysis of Structure*. Van Nostrand Reinhold: New York, 1974.
17. Safak E. Analysis of recording in structural engineering: adaptive filtering, prediction and control. *Department of the Interior U.S. Geological Survey Open File Report* 1988; 88–647.

